Current Transformer Errors and Transformer Inrush as Measured by Magnetic, Optical and Other Unconventional CTs

by
John Horak, Basler Electric Company
James Hrabliuk, NxtPhase

Classical magnetic current transformers are prone to error during a variety of conditions. The first part of this paper will identify some of those conditions and will provide a means of analyzing the resulting CT performance level. One situation of particular interest is transformer inrush current. Transformer inrush may be among the worst types of current for a magnetic CT to reproduce, because it has a combination of effects that put CT performance most at risk. Inrush may be high in magnitude, may contain a heavy DC offset with a long time constant, and it may have a unipolar half-wave nature. The paper will review the errors in secondary current that will be seen for these various primary current conditions, will provide means of determining when CTs are at risk of saturation and will show, using numerical analysis results, what the output of a saturated CT is like.

A viable alternative to magnetic CTs is the use of optical CTs that eliminate the errors commonly associated with magnetic CTs. These errors can be highly objectionable in some applications. The second part of this paper will review the various types of current sensors available on the market, including conventional, hybrid, and optical sensors. Focusing on "pure" optical sensors, the techniques used to sense current optically will also be examined, as manufacturers can use fundamentally different methods. Optical CT signals are interfaced with commercially available relays using low level analog signals and, in the near future, digital signals. These signal levels, as outlined in IEEE and IEC standards, will be examined. Finally, the future of optical sensors with respect to relaying will be examined.

Magnetic CT Performance Analysis Techniques

Steady State Circuit Analysis

The first approach to determine if a CT is under risk of CT saturation is to calculate whether the AC voltage that will be impressed on its secondary during a fault will exceed the voltage that the CT can support. This is typically done using RMS values of AC current with no DC offset.

Equivalent Electric Circuit

Most engineers have worked with CT equivalent circuits, with various modifications. The derivation and analysis is available in many references [e.g.,1]. One fairly complete version is shown in Figure 1.
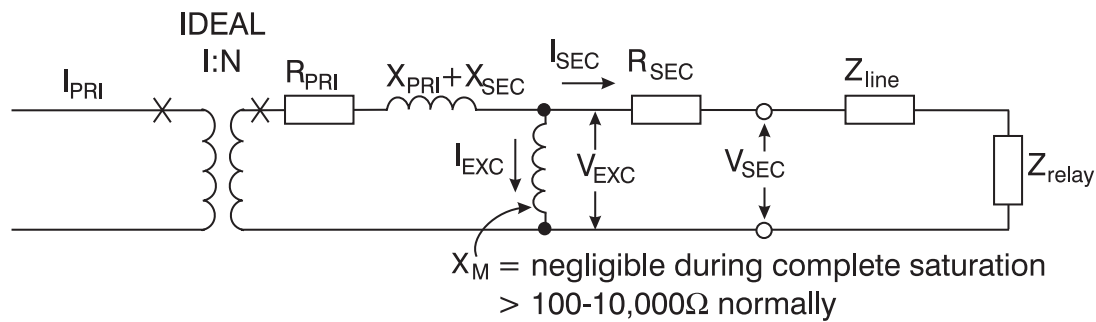
IDEAL I:N

X_M = negligible during complete saturation
> 100-10,000Ω normally

Figure 1: Simplified CT Equivalent Circuit

Note that X_m in the figure is labeled as negligible or 100-10,000 ohms (higher impedance for higher ratio CTs). The impedance of the excitation branch varies tremendously from one CT design to the next, the tap ratio used, and the V_{exc} seen by the CT. However, it is the negligible impedance during CT saturation that will most affect relay settings. This low impedance occurs when all the steel is magnetized at the steel's maximum, yet the primary current flow is oriented toward deeper magnetization. It is not until the primary current wave form decreases and eventually reverses direction that the flux level begins to reduce and saturation is removed.

CT, Line, and Relay Impedances

In Figure 1 the CT primary impedances and secondary reactance are shown but are commonly negligible. This reasonably accurate representation is used herein. However, only when a CT has "fully distributed" windings can the CT secondary reactance be considered as negligible without research. Not all CTs have fully distributed windings, but relaying class bushing CTs typically have fully distributed windings when the full ratio is used. The partial tap windings may or may not be fully distributed in old CTs.

Secondary line impedances are typically highly resistive compared to their reactance for the wire size used in CT circuits. In modern low impedance solid state relays, the burden of the relay on the CT circuit is typically negligible.

CT Secondary Voltage Rating

The impedance of the magnetizing branch is non-linear. Its approximate fundamental impedance varies with applied voltage to the CT secondary, but will typically be in the several hundred to several thousand ohms range until the saturation voltage level is reached. Note in the CT excitation curve in Figure 2 that at the indicated ANSI knee point the magnetizing impedance is 5000Ω (= 200V/0.04A). The ANSI knee point corresponds approximately to the highest magnetizing impedance of the CT. Above the knee point, small V_{exc} increases cause large I_{exc} increases, which corresponds to a low X_m.
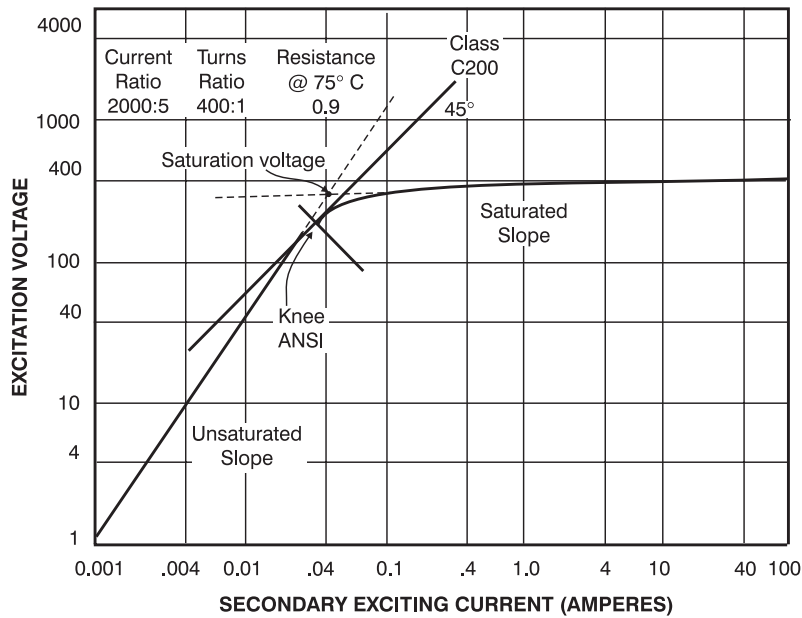
2

Figure 2: Typical CT Excitation Voltage Versus Excitation Current Curve

The steady state symmetrical AC voltage that the CT is rated to drive varies according to one's approach. Four common approaches are:

- The IEEE C57.13 "knee point" for ungapped core CTs, constructed using the intersection of the excitation curve and a 45° line as shown in Figure 2. (Gapped core CTs use 30° but are not common in relay circuits.)
- The "saturation voltage" using the intersection of straight lines drawn from the two sections of the curve as shown in Figure 2.
- The IEC knee point defined as the voltage where a 10% increase in V_{exc} will cause a 50% increase in I_{exc}.
- The "C" rating of the CT (IEEE C57.13). The C rating calls for less than 10% relay current error at 20 times rated current (5*20, or 100A) into 1, 2, 4, or 8Ω 0.5pf burdens. A simplified method, that ignores phasor math, for determining the C rating for a 5A CT from the curves:

1) Find V_{exc} where I_{exc}=10. Note V_{exc} is an internal voltage, not the CT terminal voltage.

2) Now calculate the CT terminal voltage with this V_{exc} and 100A secondary (100A is measured secondary, but we can see we lost 10A to the excitation branch, so we have an error of 10/(100+10)=0.091, or less than 10% error).

$$V_{ct,terminal} = V_{exc} -100(R_{ct}).$$

3) Round $V_{ct,terminal}$ down to the nearest 100, 200, 400, or 800V, corresponding to C100, C200, C400, and C800 (C10, C20, and C50 CTs are also sold, but

3

their design pf burden may be 0.9).

As an example, from the above curves, with a 0.9Ω secondary:
$$V_{ct,terminal} = 400 - 100(0.9) = 310V, \text{ which yields C200 rating.}$$

The sample CT in Figure 2 has an ANSI knee point of about 200V, a saturation voltage of about 275V, and is class C200.

Steady State AC Saturation

The next step is to apply anticipated faults to the system and determine if the voltage that will be impressed upon the CT will be greater than the CT rating:

$$V_{CT,Rated} \geq K \cdot I_{sec,rms} \cdot Z_{sec} \qquad \text{Eq. 1}$$

where

$V_{CT,Rated}$ = Knee Point, Saturation Voltage, or C Rating, depending on the user's decision

K = User's Safety Margin Factor

The equation must be evaluated for all likely CT secondary current distributions for phase and ground faults, verifying that the CT will not see excessive secondary voltage during the fault. Some common situations where problems arise:

- Impedance is too high due to long lead lengths.
- Poor quality (i.e., low burden rating) CTs are used due to cost constraints or space limitations.
- Small loads are placed on powerful buses, and CT ratios are selected based on load current rather than fault duty.
- Low ratio zero sequence CTs are placed on systems having high ground fault duty.
- Unusual burdens, such as differential relay stabilizing resistors, are placed in the CT circuit.

Transient Analysis of Inrush and Fault Current

The effect of DC offset, unipolar half wave current, and residual flux in the CT can almost always cause at least a small amount of transient CT saturation in a CT that is otherwise totally acceptable for steady state AC fault current. All these components will be found in transformer inrush current.

Simple Approach – Integration of Ideal CT Secondary Voltage

The analysis of CT flux levels under the presence of a mix of symmetrical AC and other non-symmetrical current wave forms, especially if any modeling of CT saturation is to be included, is a rather involved process. A simplified test of whether a CT is at risk of entering saturation under the presence of DC offset or unipolar current waves is to integrate secondary voltage as if the CT were ideal.

4

To provide voltage in a circuit requires a changing flux level in a coil:

$$V = \frac{d\lambda}{dt}$$

Eq. 2

By integrating the voltage at the terminals over time we can determine the core flux level:

$$\lambda(t) = \int_0^t V\,dt + \lambda_o$$

Eq. 3

where λ_o = residual flux level at time 0

This equation provides a measure of the rating of a CT. At rated secondary voltage and no standing offset from 0, the flux that the CT can produce is simply the integration of

$$\lambda = \int \sqrt{2}\,V_{rms,rated}\,\sin(\omega t)\,dt$$

$$\lambda_{peak} = \frac{\sqrt{2}}{\omega} V_{rms,rated}$$

Eq. 4

If the integration of secondary voltage rises above this level, then the CT begins to saturate.

Simplified Analysis of DC Offset Effects

Faults develop an AC current with an exponentially decaying DC offset that is expressed by the following equation developed in many engineering texts (e.g. [2] chapter 3):

$$I_{pri}(t) = \left(\frac{\sqrt{2}\,V_{rms,pri}}{\left|R_{pri} + jX_{pri}\right|}\right)\left(\sin(\omega t + \alpha) - \sin(\alpha)\,e^{-tR_p/L_p}\right)$$

Eq. 5

where

$$R_p / L_p = R_{pri} / (X_{pri} / \omega)$$
$$\omega = 2\pi f$$

α = a function of system X/R and where in the cycle the fault is initiated. Randomly takes any angle.

By assuming that the CT secondary burden is a pure resistance, assuming an infinitely permeable core, and assuming the worst case DC offset by setting $\alpha = -\pi/2$ ($+\pi/2$ would be just as bad), the voltage impressed on the CT secondary will have the form of:

$$V_{sec}(t) = \sqrt{2}\,I_{rms,pri}\left(\frac{R_{CTburden}}{CT\,Ratio}\right)\left(\sin(\omega t - \frac{\pi}{2}) + e^{-tR_p/L_p}\right)$$

Eq. 6

Inserting Eq. 6 into Eq. 2 yields:

$$\lambda(t) = \sqrt{2}I_{rms,pri}\left(\frac{R_{CTburden}}{CTRatio}\right)\left[\left(-\frac{1}{\omega}\cos(\omega t - \frac{\pi}{2})\right) + \left(\frac{L_p}{R_p}\left(1 - e^{-tR_p/L_p}\right)\right)\right] + \lambda_o \qquad \text{Eq. 7}$$

Examination of Eq. 7 shows that, the higher either fault current or burden, the higher the voltage and the higher the flux level. Figure 3 is a graph of the results of the above analysis, showing the flux buildup that will occur in a CT during an event, assuming a pure resistive secondary circuit and an infinitely permeable core.
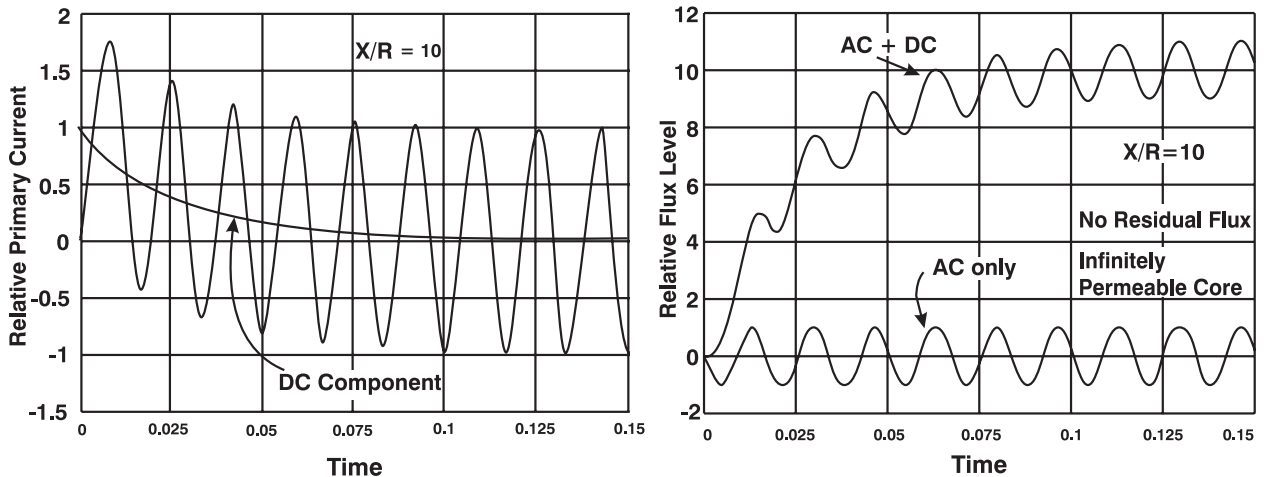

Figure 3: CT Flux Levels with DC Current Effects, Infinitely Permeable Core

Figure 3 does not show any residual flux at the start of the process. All practical magnetic cores hold some level of flux after current is removed, and during normal operation a CT may reproduce an AC waveform with core flux levels that are constantly offset from a zero flux level. The offset tends to be worst immediately after a major reduction in current levels and tends to decrease with time. High speed reclosing sees larger flux offsets as a result, which tends to cause worse transient CT saturation. In a sample test reported in [1], the residual flux level found in a variety of CTs varied over the range of 0-80% of design flux level. About half of the CTs had residual flux levels above 40% of rated. Residual flux may be oriented in either direction. Hence, the flux indicated in Figure 3 may be shifted up or down depending on the level of residual flux.

Core flux levels, of course, do not reach the levels shown in Figure 3. The core reaches a level of flux density and flux levels do not appreciably increase after that point. Thereafter, the CT output drops toward zero in an exponentially decaying fashion until primary current flows in the negative direction to desaturate the CT. As the DC offset decays, the CT output gradually improves until the secondary current represents the input waveform.
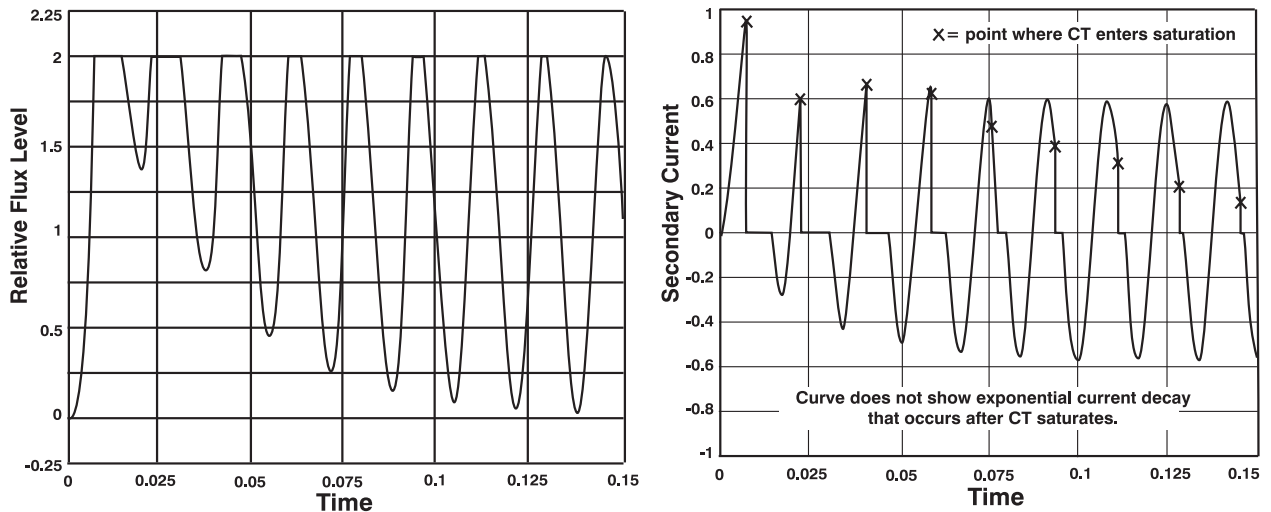
Figure 4: Simplified Saturation Effects Analysis

It would be possible to provide "time to saturate" and "time to desaturate" equations, but this is not done herein, because exact times are not the point of this exercise and likely a fairly inexact analysis due to unknown circuit impedances, CT magnetic approximations, and pre-event flux levels. (Equations may be found in [1] and [3].) The point here is:

1) Saturation may occur very quickly, as fast as the first half wave of the primary current wave, and

2) Given a saturated CT, as the primary current DC offsetdecays, the output waveform returns to a normal AC waveform. Note that, as shown in Figure 4, after 0.1 seconds (about two system time constants; T.C.=L/R=X_L/(ωR), or about 0.053 seconds for X/R =10), the output wave form has begun to look closer to the normal AC wave form.

Peak Flux Assuming No Saturation

By substituting into Equation 8 for some time well into the future when the exponential DC offset term has essentially been completely integrated, and choosing a point in time where the cosine term comes to 1, we can state the peak flux if there is no CT saturation:

$$\lambda_{max} = k\left[\left(\frac{1}{\omega}\right)+\left(\frac{L_p}{R_p}\right)\right]+\lambda_o$$

Eq. 8

Comparing the max flux level with and without the *L/R* term, noting *x = 2π fL=ωL*, and dropping the initial flux term λ_o , we can see a ratio of maximum flux with and without the DC offset:

$$\frac{\lambda_{max,dc+ac}}{\lambda_{max,ac}}=1+\frac{X_{L,p}}{R_p}$$

Eq. 9

7

Where

$$\lambda_{max,dc+ac} = \text{the peak flux level that would arise from a secondary voltage with}$$
$$\text{both an ac and dc component, and no residual flux effects}$$
$$\lambda_{max,ac} = \text{the peak flux level that would arise from a secondary voltage with}$$
$$\text{only an ac component, and no residual flux effects}$$

Recall that this X_L/R value refers to the fault impedance of the primary circuit, typically on the order of 3-15. This means that to avoid saturation due to DC offset, the CT must have a voltage rating that is 4-16 times the voltage rating required for the steady state AC analysis, ignoring the effects of residual flex levels.

DC Offset Analysis Conclusions

From the discussion above, we can conclude that, to avoid all hints of saturation from the effects of DC offset (but ignoring residual flux effects), we need to revise equation 1 to say:

$$V_{CT,Rated} \geq K\left(1 + \frac{X_{L,p}}{R_p}\right) \cdot I_{sec,rms} \cdot Z_{sec} \qquad \text{Eq. 10}$$

where K is some margin/safety factor to account for uncertainties, such as the effects of residual flux and circuit modeling error.

Simplified Analysis of Unipolar Half Wave Currents

Transformer inrush currents are frequently characterized by a half wave current that has the appearance of the output of a half wave voltage rectifier. From the above analysis of DC offset effects on flux build-up, it becomes clear that any time the integration of secondary voltage exceeds the design rated volt-second rating of the CT, the CT is at risk of entering saturation. The negative half of a current wave is needed to balance the positive voltage waves and, if the waves are not balanced, the integration of secondary voltage will build and the CT will enter saturation. The number of unipolar pulses that the CT can reproduce before entering risk of saturation is a straightforward matter. Simply add the area under the voltage profile curves of an ideal CT until the integration reaches the voltage rating defined by eq. 4. Depending on secondary voltages and the CT rating, the CT is at risk of going into saturation even during the second pulse of the half wave rectified current.
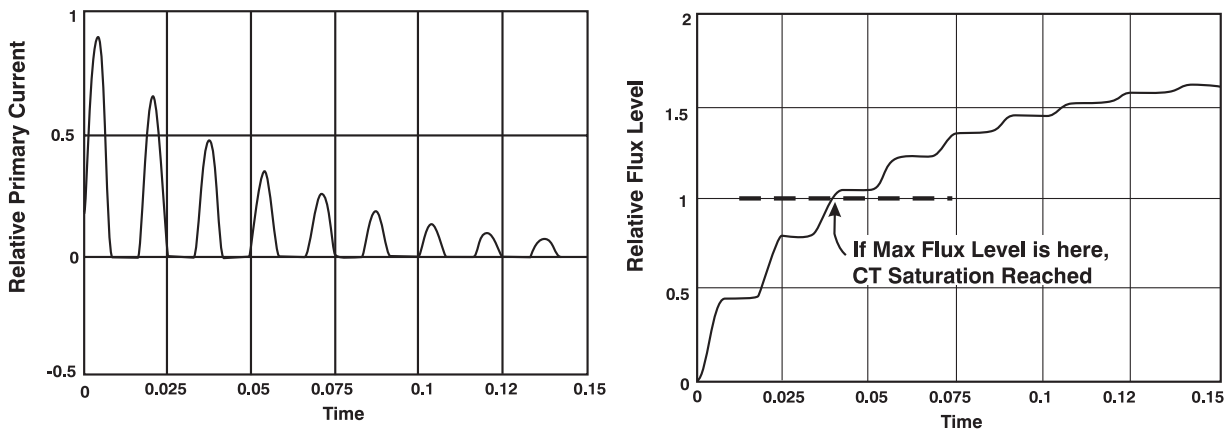
Figure 5: Point where CT saturation is reached

Detailed Numerical Analysis of Saturated Conditions

The classical model is mainly for the purpose of modeling steady state AC performance during normal unsaturated conditions and minor excursions into the saturated domain. It is not well suited for modeling conditions that tend toward moderate to heavy CT saturation. Also, the above analysis of the integration of CT secondary voltage gives an indication of when a CT is at risk of entering saturation, but it does not lend itself to a good description of what the CT output will actually look like when saturation does occur. Once a CT is suspected to be operating at moderate or heavy saturation levels, or when the effects of minor contributors to inaccuracy, such as hysteresis, are of interest, a numerical analysis of the CT currents, voltages, and magnetic circuits is required. See the appendix for one method of numerical analysis of CTs.

CT Driven into Saturation by Excessive Burden or Primary Current

If a CT is driven by too much primary current or excessive secondary burden, the CT will begin to have an output similar to Figure 6. This figure represents the possible case where a 5MVA, 13.8kV transformer was installed on a 10,000A bus. A 600:5 CT was used, tapped closer to the system load of 200A, so the C200 CT became a C65. This might be fine for typical load currents, but when a major fault occurs (that would have in theory driven 250A into the relay), the CT fails, and it is hard to predict how a relay will respond to such a distorted wave. Even if the CT had not failed, it is not immediately clear how the digital relay will respond to currents of such magnitude. The analog to digital circuits and front end op amps likely saturate, and a distorted current wave is seen by the relay.
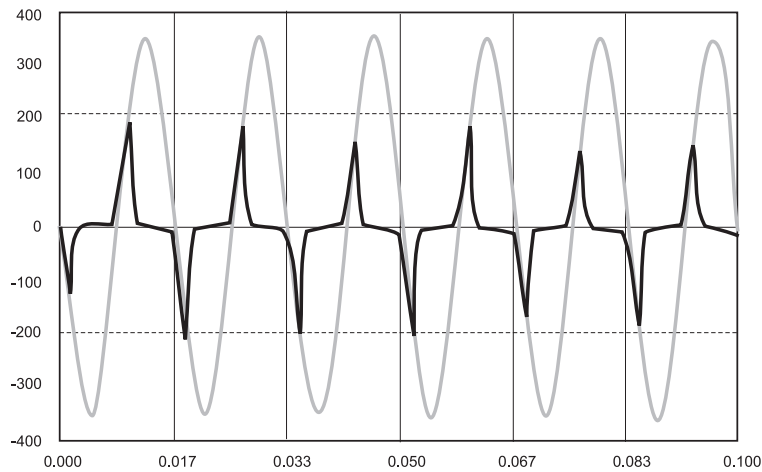
Figure 6: 600:5 tapped at 200:5; C200 effectively a C65; 1.2+j.2 Ω burden total

CT Driven into Saturation by Heavy DC Offset in Inrush or Fault

Now take the previous example, and assume that the CT was tapped at 600:5, so the CT could reproduce the primary current relatively well, but a large DC offset was present in the wave and the steel of the CT had some level of offset. This will cause a transient saturation. The distorted waveform occurs. Again, it becomes hard to predict what will occur in the relay. Overcurrent relay response will slow, but differential relays may tend toward misoperation.
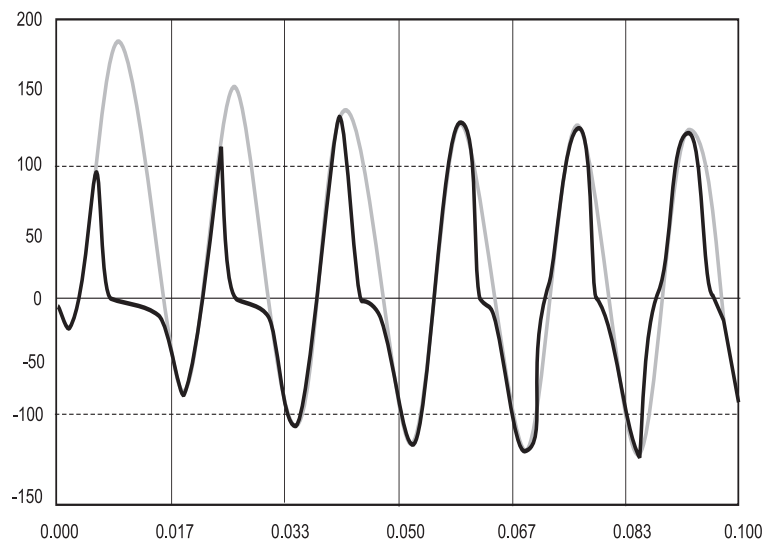

Figure 7: Same CT, tapped at 600:5, but with heavy DC offset

CT Driven Into Saturation by Unipolar Transformer Inrush

Inrush current driven that is half-wave-like in nature will eventually drive a CT into saturation. As noted in the earlier graphs, it will cause a cumulative buildup of flux and, if extended long enough, will cause a CT to fail to reproduce current and, hence, cause another unexplained operation of the transformer differential relay.

10

Current Sensing Using Optical CTs

Within the past ten years optical sensors have seen greater acceptance, to the point that designers have a viable alternative to conventional instrument transformers. This shift toward optical technology is being driven by improved safety, accuracy, broader dynamic range, wider bandwidth, reduced size, and the use of environmentally friendly materials. For protection applications specifically, optical current sensors can represent the true primary current flowing on the line, eliminating the problems of CT saturation. This signal representation can also represent "pure DC" or "DC components" flowing on the line.

Optical sensor manufacturers use fundamentally different techniques to measure current and, in many cases, the physical constructions are very different. Even the term "optical sensor" can be confusing, as sensors using non-optical methods of measuring current (but using an optical method of transmitting the signal) fall under the new IEEE and IEC standards. In contrast, various manufacturers' conventional instrument transformers are generally built using the same fundamental technology: iron core with a copper winding transformer. It can be confusing for users trying to evaluate the benefits of optical sensors; one must understand not only the differences from conventional devices, but also the various approaches to optical sensing.

The current sensor "family tree" shown in Figure 8 clarifies the various types of current sensors available. These sensors can be divided into two broad classes, conventional sensing and optical sensing. "Optical" can have several different meanings; this family tree refers to optical sensing as "pure" optical sensors that use optical materials and fundamentally different techniques to measure current.

Some current sensing methods use conventional iron core or novel current sensing techniques, and then convert the conventional analog signal into an optical signal that is then transmitted to remote electronics. These types of sensors are referred to as "hybrid" optical sensors.

Focusing on "pure" optical sensors (measure and transmit the signal optically) there are several distinct methods of measuring the current. These techniques vary in both the physical construction of the sensor and the overall measurement technique, which may be patented by the specific manufacturer. Understanding those differences is critical to optical sensor selection.
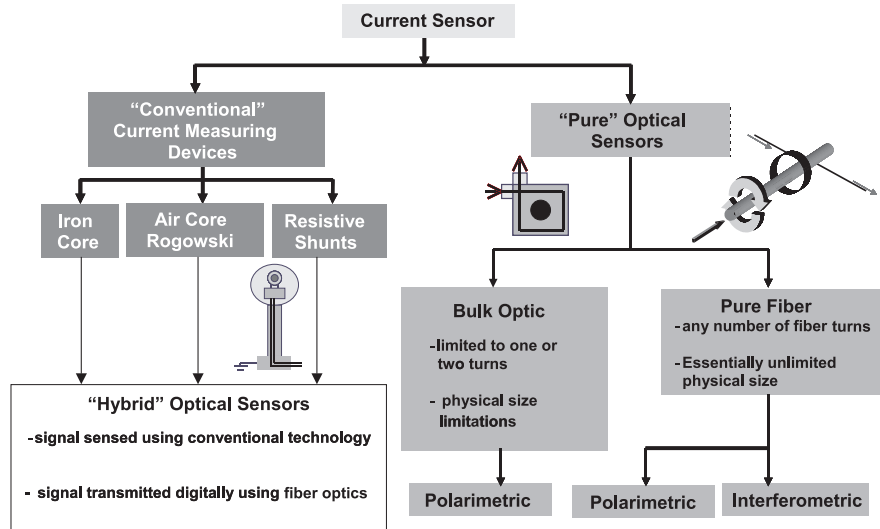
Current Sensor "Family Tree"

Figure 8: An overview of major categories of current sensing approaches on the market

Types of Optical Current Sensors

Within the "pure" optical sensor category, sensors can be broadly categorized as using "bulk optics" or "pure fiber optics". "Pure" fiber sensors use fiber wrapped around a current-carrying conductor and are able to use any number of fiber turns surrounding the conductor. Depending on the measurement technique and, hence, the physical properties of the components, the sensor can be manufactured in a wide variety of physical shapes and sizes. This flexibility can allow CTs of very large physical size to be manufactured (for example, for bushing CTs). Bulk sensors, on the other hand, use a block of glass machined to direct light around the conductor, limiting its ability to adapt to various shapes and sizes.

Polarimetric vs. Interferometric Sensing

Looking even closer at fiber optic devices, they may be further classified as "polarimetric" and "interferometric" sensors. Polarimetric and interferometric sensing are fundamentally different in their sensitivity to stray effects such as temperature and vibration.

Polarimetric current sensors derive measurements from a shift in the "polarization of light" caused by the magnetic field surrounding a current-carrying conductor. Linearly polarized light enters the sensor, where its polarization is shifted by an amount proportional to the magnetic field (and proportional to the amount of current flowing through the line). Stray effects shift the polarization of the light and make it difficult to determine the actual current in the conductor. Mitigation of these stray effects becomes critical to the success of the sensor's accuracy and stability. Elimination of these effects is accomplished through delicate packaging of the optics and compensation techniques. These mitigation procedures are limited in their effectiveness and, in turn, limit the performance of the polarimetric sensor.

An interferometric sensor derives the measurement of current from the "interference of waves" caused by a phase shift between two lightwaves. This interference is the result of two circularly polarized light signals whose speeds of propagation are altered "differentially" in proportion to the magnetic field induced by the current in the conductor. External temperature and vibration, which are "common mode" effects, equally affect the light signals; therefore, the sensor is relatively immune to these stray effects.
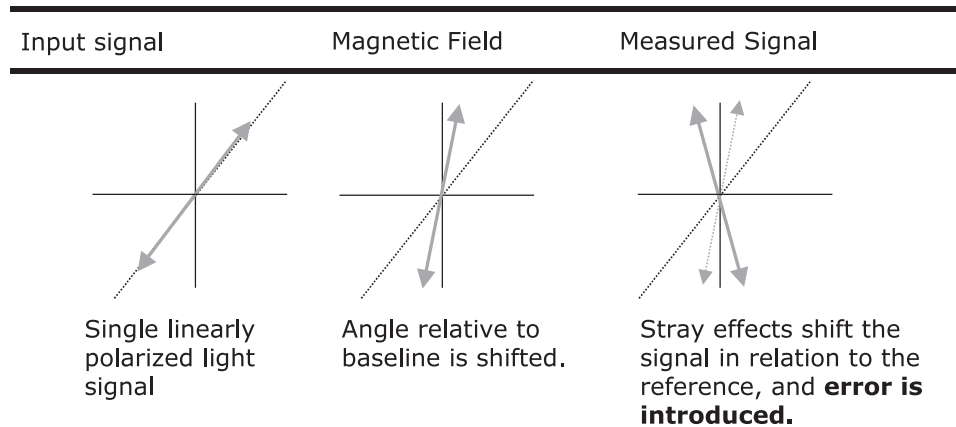
Input signal	Magnetic Field	Measured Signal
Single linearly polarized light signal	Angle relative to baseline is shifted.	Stray effects shift the signal in relation to the reference, and **error is introduced.**

Figure 9: Polarimetric CTs measure the magnitude of a shift in the polarization of light caused by the current in a conductor.
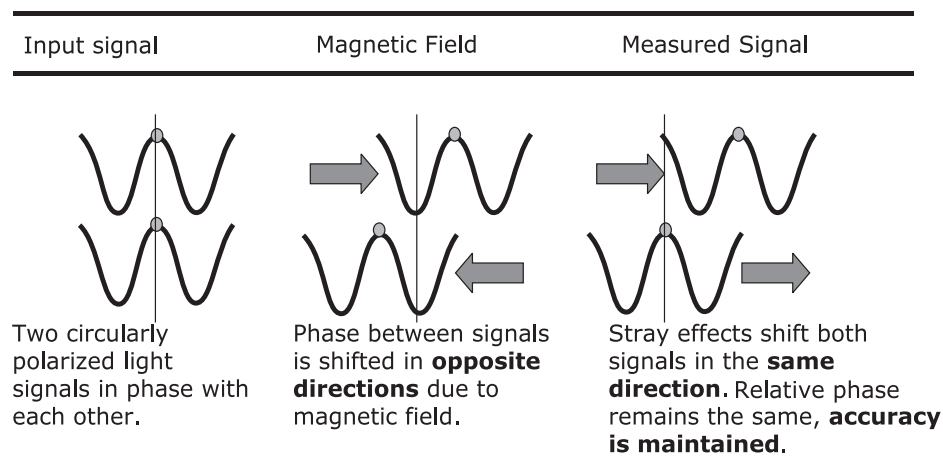
Input signal	Magnetic Field	Measured Signal
Two circularly polarized light signals in phase with each other.	Phase between signals is shifted in **opposite directions** due to magnetic field.	Stray effects shift both signals in the **same direction.** Relative phase remains the same, **accuracy is maintained.**

Figure 10: Interferometric CTs measure the difference between polarization shift of two signals caused by the current in a conductor.

An Interferometric Design

One specific current sensor utilizes the Faraday[1] effect in a unique manner; the magnetic field produced by the current flowing through a conductor changes the velocity of the circularly polarized light waves in the sensing fiber. By measuring the change in light velocity (using an interferometric scheme) and processing the information, an extremely accurate measurement of current is produced.

[1] The Faraday, or magneto-optic effect, consists of the rotation of the polarization plane of an optical wave, traveling in a magneto-optic material, under the influence of a magnetic field parallel to the direction of propagation of the optical wave.

This approach to current sensing has been adapted from a completely different industry. Used for years in navigation systems, the design is based on the Honeywell fiber-optic gyroscope system. In the 1990s, a team of spin-off researchers at Honeywell investigated the measurement of electrical current using fiber-optic gyroscope technology developed earlier for civil and military navigation applications. This early development led to the use of this technology for application in current sensing and in measurement devices for power system monitoring. The method is detailed below.
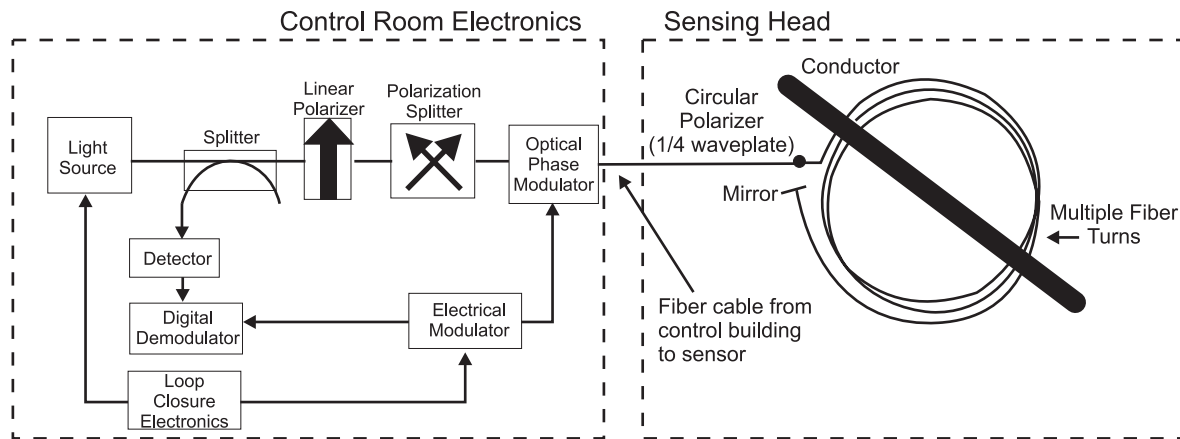

Figure 11: Fiber optic current sensing technology. Circularly polarized light travels in both directions around the fiber loop with speed of propagation differentially influenced by the Faraday effect. The signal is normalized and bifurcated with a modulator and closed loop electronics to yield a highly accurate current measurement impervious to temperature and vibration effects.

1. A light source sends light through a waveguide to a linear polarizer, then to a polarization splitter (creating two linearly polarized light waves), and finally to an optical phase modulator.

2. This light is then sent from the control room to the sensor head by an optical fiber.

3. The light passes through a quarter waveplate, creating right and left hand circularly polarized light from the two linearly polarized light waves.

4. The two light waves traverse the fiber sensing loop around the conductor, reflect off a mirror at the end of the fiber loop, and return along the same path.

5. While encircling the conductor, the magnetic field induced by the current flowing in the conductor creates a differential optical phase shift between the two light waves due to the Faraday effect.

6. The two optical waves travel back through the optical circuit and are finally routed to the optical detector where the electronics de-modulate the lightwaves to determine the phase shift.

7. The phase shift between the two light waves is proportional to current, and an analog or digital signal representing the current is provided by the electronics to the end user.

Optical CT Installation

Figure 12: Installation of optical voltage and current sensors at a gas-turbine generating station.

Interfacing Optical CTs with Relays

Those who specify conventional current transformers use IEC and IEEE standards to assist in the writing of a specification. With the addition of optical current (and voltage) sensors, new standards were required to address these new devices. The IEC has been a leader with respect to development of these standards, with the IEEE following closely behind. The new optical standards are very similar with respect to "high voltage" and accuracy; although, in some instances, the sensors are tested to more stringent standards. These more stringent tests include accuracy over temperature and additional EMC tests for the electronics. Additionally, the optical sensors (and their associated electronics) must comply with existing standards previously associated with electronic relays or meters.

When specifying optical sensors, the new standards should be used to specify the performance of the sensor, since various new signal outputs are available. High voltage and high current requirements are the same for optical sensors as for conventional equipment. These tests have evolved over many years, and the standards are not intended to modify them; they are tested and proven. The standards for conventional and optical sensors are summarized below into two groups: conventional standards that have been in print for many years, and optical standards that are relatively new and unfamiliar to most people.

Signals representing current from optical sensors are typically available in three formats: digital, low energy analog (LEA), and high energy analog (HEA) for metering applications only. The fundamental signal is the digital signal. It is this digital signal that has the greatest value, as it does not require the additional complexity of digital to analog conversion nor does it require amplification of a low energy analog signal. However, given that digital signal inputs to meters and relays are in early stages of development, high and low level analog signals are available in the interim until digital inputs to secondary devices are more commonly available.

15

Digital Signal

Signal processing inside the current and voltage electronics is inherently digital in nature and is accessible in a format consistent with IEC standard 60044-7 and draft standard 60044-8. These standards define the digital data format from the sensor electronics (contains the relevant signal information associated with several current and voltage sensors). In addition, IEC 61850-9-1 and 61850-9-2 also recognize the data structure outlined in the 60044-7 and 60044-8 standards, but also permit an Ethernet physical layer with the same overall data structure.

Low Energy Analog (LEA) Signal

A low energy analog (LEA) signal from each sensor is available in several formats, each tailored to its specific sensor and end use. The table below summarizes output signals and applicable standards (in some cases, draft standards):

Low Energy Signal Levels Available

	Current Sensor	Voltage Sensor
Metering Output	$4V_{RMS}$ (meets IEC 60044-8) $2V_{RMS}$ (ANSI/IEEE PC37.92)	$4V_{RMS}$ (meets IEC 60044-7)
Protection Output	$200\ mV_{RMS}$ (meets IEC 60044-8 and ANSI/IEEE PC37.92)	$4V_{RMS}$ (meets IEC 60044-7 and ANSI/IEEE PC37.92)

These signal amplitudes were chosen based on widely acceptable output levels from digital to analog converters with a maximum output voltage of approximately 11.3 V_{peak}. IEC and IEEE standards allow for an over range factor of two for metering on the voltage and current outputs and 40 for the protection current output. (This permits measurement of a fully offset waveform with a magnitude of 20 times rated current as outlined in the standards, while maintaining the maximum peak signal level below 11.3V.)

High Energy Analog (HEA) Signal

The high energy analog signal is available in a format that typically would be used for metering applications. Amplifying a current signal to be used for protection applications is possible but is impractical, because the required over range for fault currents would require a very large and expensive amplifier. Low energy signals are more suitable for relaying applications. For similar reasons a 1A signal (but not a 5A signal) is available for metering applications. The table below summarizes the available high energy analog signals:

High Energy Signal Levels Available

	Current Sensor	Voltage Sensor
Metering Output	1 A_{RMS}, 2.5VA burden typical	69 or 115 V, 2.5VA burden typical
Protection Output	N/A	N/A

Relevant Standards

IEC 60044-7: Instrument Transformers – Part 7: Electronic Voltage Transformers

IEC 60044-8: Instrument Transformers – Part 8: Electronic Voltage Transformers

ANSI/IEEE PC37.92 Standard for Low Energy Analog Signal Inputs to Protective Relays

IEC 61850-9-1: Specific Communication Service Mapping (SCSM) – Serial Unidirectional Multidrop Point to Point Link

IEC 61850-9-2: Specific Communication Service Mapping (SCSM) – ACSI Mapping on an IEEE 802-3 based Process Bus

Optical CT Performance During Fault Condition

Type testing of an optical current sensor illustrates an ability to accurately measure high fault currents. An optical current sensor tested with a fully offset waveform and a magnitude of 108 kA_{peak} (40kA_{RMS}) is shown in Figure 13. Linearity of the optical sensor as compared to a precision resistive shunt is better than 2%.
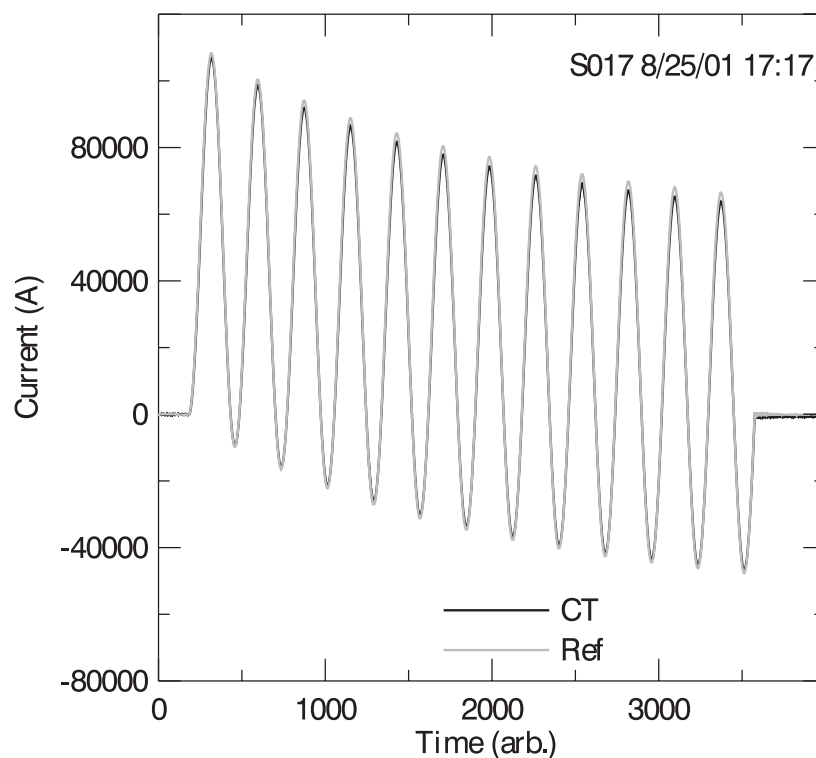

Figure 13: Fully Offset 40kA_{RMS}, 108kA_{peak} Fault Currrent – 12 Cycle Duration

A symmetrical fault current with magnitude of 40 kA_{RMS} is shown in Figure 14 compared with a precision resistive shunt. A 3 cycle accuracy test at this fault current of 40 kARMS had errors less than 2%, far exceeding both IEEE and IEC standards.
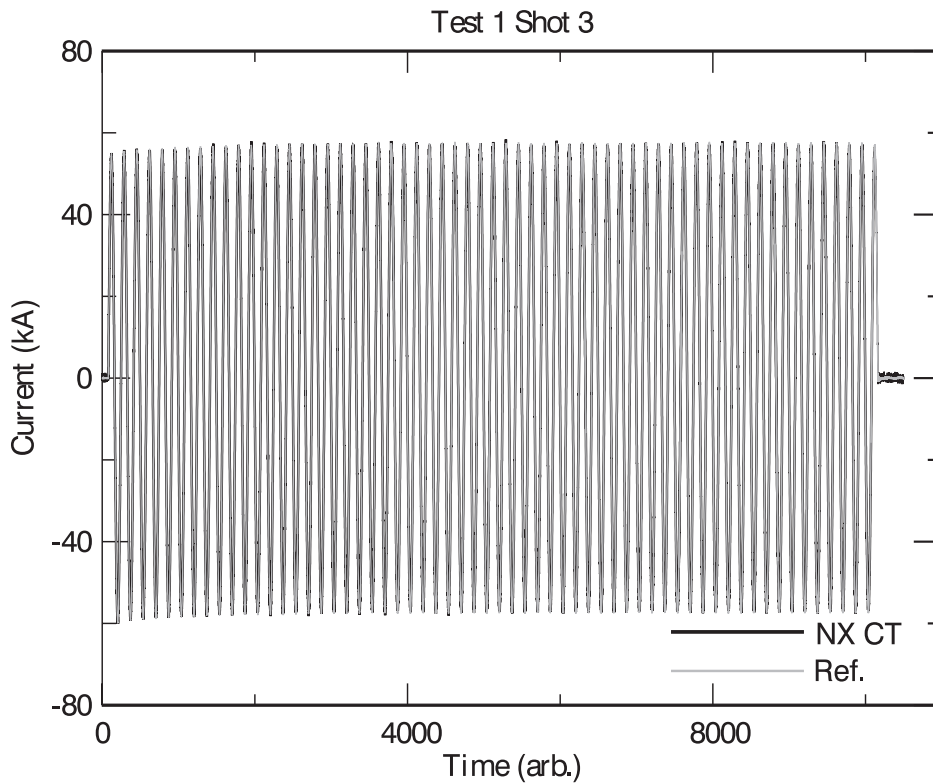
17

Figure 14: Symmetrical 40kA$_{RMS}$ Thermal Fault Currrent Test – One Second Duration

The Future of Optical Sensors

Optical sensors could truly revolutionize our industry. With an inherent digital signal, optical sensors can be utilized in ways that are not possible with conventional analog signals. Imagine an all-encompassing digital substation with voltage and current sensors, relays, meters, controls, SCADA functions, breakers, and switches. Many possibilities exist to streamline design, maintenance, testing and commissioning within a substation.

Additionally, optical sensors have associated electronics that can alter the fundamental characteristics of the measurement system via software. No longer is the characteristic of the sensor determined and fixed after leaving the manufacturer's factory door. Generic optical sensors can be "user customized" through software to optimize a user's specific application. The improved measurement capabilities and system flexibility associated with the inherent digital sensors are tremendously powerful for users.

For example, one of the most challenging situations for conventional CTs is the combination of small load currents with high fault currents. In these situations, the conventional CT ratio must be selected to ensure limited saturation during fault conditions and to limit secondary currents from exceeding specifications of relay input circuits. In an optical sensor no such limitation exists, since there is no mechanism for saturation, and the output of the electronics cannot achieve damaging current levels. The electronic signal output is available digitally and is also available in an analog output configured to 200 mV. Similarly, when fault currents creep up in the power system, the CT ratio can be changed using a laptop computer (as applied by existing microprocessor based relays) to accommodate the new fault levels. Configuration can be completed without changing CTs or modifying

18

wiring. In the future, configuration could even be done in real time, analogous to a "setting group" change on a relay.

Relay testing is also an important example. In fact, relay testing as it is presently known could change radically. Present methods of testing relays involve the creation or capture of signals that are then "played back" into relays to test their response. This process of testing requires the creation or capture of a digital file (such as a COMTRADE) with the desired test signals. These files, containing the "digital signals", are then converted into an analog signal, followed by amplification of the analog signal to commonly accepted "secondary" values such as 5A and 69V. This process of "playing" the desired signals into a relay to test the response, when examined in detail, is very cumbersome. Designers must purchase and design test switches into the relaying system, and those switches are then installed in panels by construction or maintenance crews. Depending on the relay testing philosophy of the utility, maintenance is then scheduled and performed on a periodic basis to verify the functionality of the relay. This requires the technician to walk, drive, fly and sometimes even boat into the substation site. Bulky equipment capable of reproducing the 5A and 69V secondary signals must be brought to site, the relay taken out of service and tested. This entire process could be simplified if the initial digital file could be executed over a network in the substation. Physical test switches could be eliminated. Fault records captured by relays could be stored and played back into other relays on the network automatically. Test equipment would be greatly reduced, if not eliminated, moving towards software based testing. Optical sensors with digital outputs, which are given to relays with digital inputs, can drive this vision to reality. Visions such as this are no longer futuristic; they are now on the immediate planning horizon.

Protection Outputs

One of the more difficult situations to design for when using conventional CTs occurs when load currents are small and fault currents are high. In such a situation, the conventional CT ratio must be selected to ensure limited saturation during fault conditions and to limit secondary currents from exceeding specifications of relay input circuits. In an optical sensor, no such limitation exists since there is no mechanism for saturation, and the output of the electronics cannot achieve damaging current levels. The electronic signal output is available digitally and is also available in an analog output configured to 200 mV. Similar to when load currents increase, when fault currents creep up in the power system, the CT ratio can be changed using a laptop computer, similar to existing microprocessor based relays, to accommodate the new fault levels. This can be done without changing CTs or modifying wiring and, in the future, could even be done in real time analogous to a "setting group" change on a relay.

Optical current sensors, in principal, perform the same function as conventional magnetic CTs; they measure current. However, optical sensors are not the industry norm and, when comparing them with magnetic devices, it can be confusing. Many of the terms and definitions associated with conventional magnetic sensors have no relevance to optical sensors; they require their own "language" that must be learned.

REFERENCES

[1]   IEEE C37.110 (1996), IEEE Guide for the Application of Current Transformers Used for Protective Relay Purposes

[2]   Allan Greenwood, <u>Electrical Transients in Power Systems, Second Edition,</u> John Wiley & Sons, 1991

[3]   "Transient Response of Current Transformers," Power System Relaying Committee Report 76-CH1130-4 PWR, IEEE Special Publication, 1976

[4]   IEC 60044-7: Instrument Transformers – Part 7: Electronic Voltage Transformers

[5]   IEC 60044-8: Instrument Transformers – Part 8: Electronic Voltage Transformers

[6]   ANSI/IEEE PC37.92 Standard for Low Energy Analog Signal Inputs to Protective Relays

[7]   IEC 61850-9-1: Specific Communication Service Mapping (SCSM) – Serial Uni-directional Multidrop Point to Point Link

[8]   IEC 61850-9-2: Specific Communication Service Mapping (SCSM) – ACSI Mapping on an IEEE 802-3 based Process Bus

BIOGRAPHIES

John Horak is an Application Engineer for Basler Electric. Prior to joining Basler in 1997, John spent nine years as an engineer with Stone and Webster, performing electrical design and relaying studies, which included six years on assignment to the System Protection Engineering unit of XCEL Energy. Prior to joining S&W he spent three years with Chevron and Houston Light and Power. He earned a B.S.E.E. from the University of Houston and an M.S.E.E. in power system studies from the University of Colorado. Mr. Horak is a member of IEEE PES and IAS and a Professional Engineer in Colorado.

James Hrabliuk was born in Dauphin, Manitoba, in 1967. He received his B.S.E.E. from the University of Manitoba in 1989. His experience includes 12 years at Manitoba Hydro designing transmission substations and protection systems. In March 2000, he joined NxtPhase Corporation of Vancouver, B.C., as an applications engineer. Mr. Hrabliuk is a member of the Association of Professional Engineers and Geoscientists of British Columbia (APEGBC) and the Institute of Electrical and Electronics Engineers (IEEE).

APPENDIX -- Magnetic Saturation and CT Modeling Theory

Magnetization Curve

A method of CT modelling is given below. It includes a modified version of the Jiles and Atherton (J-A) model for magnetic circuit hysteresis and permeance [1, 2]. It has been modified to reflect data that is commonly available on CTs. The J-A approach to magnetic path analysis considers the steel magnetic flux to consist of two parts: a) an anhysteretic B-H flux component, and b) a hysteretic flux component where flux is 'sticky' and changes only after the H field reaches a threshold.

Anhysteretic Flux Component

An "anhysteretic" flux function refers to a "single valued" function where, given *H* field, there is only one possible corresponding *B* field in the steel. An anhysteretical function has no hysteresis and no remnant flux. Jiles and Atherton used a variation of a hyperbolic cotangent function to represent the anhysteretical flux component. However, it is not a straight-forward "plug-in-and-go" process to determine the constants for the J-A model from a typical $V_{exc,rms}$-$I_{exc,rms}$ curve. A function that can more easily be set up will be provided below.

The excitation data most commonly supplied by CT manufacturers are $V_{exc,rms}$-$I_{exc,rms}$ curves. However, exact B-H curves cannot be determined from this data, mainly because the RMS nature of the data involves an integration of a possibly non-sinusoidal data over at least a cycle, and hence hides instantaneous λ and i data. Also adding confusion, the curve provides voltage against current. Voltage is a derivative of rate of change of flux, so flux magnitude is only inferred and the initial value of flux is difficult to determine.

If it is assumed that $V_{exc,rms}$-$I_{exc,rms}$ curves are generated by the CT manufacturer with a pure sine wave voltage, and that at voltages below the saturation levels the excitation current is mainly a fundamental frequency phenomena:

$$\lambda_{peak} = \frac{\sqrt{2}}{\omega} V_{rms}$$

$$i_{peak} \approx \sqrt{2}\, I_{rms} \quad (\text{below } V\text{-}I \text{ knee})$$

Eq. A1

This allows for an approximation of the λ-i curve directly from the $V_{exc,rms}$-$I_{exc,rms}$ in the area below the CT knee point. Since excitation current in this area is very small relative to typical CT loading, the error from assuming a sine wave excitation current has a minor effect on performance evaluation.

Above the CT saturation knee point, the excitation current becomes large and begins to have increasingly large odd harmonic components and a 'peaky' waveform. Hence, the approximation that $i_{peak} = \sqrt{2} \cdot i_{rms}$ is no longer valid. In [4] there is a development of estimating the excitation current in the saturated region as an exponential curve. (As [4] has not been formally published yet, the logic will be covered only briefly.) An examination of typical $V_{exc,rms}$-$I_{exc,rms}$ curves shows that above the knee point,

$$\log V_{exc} = S \log(I_{exc}) + \log(V_1)$$

$$V_{exc} = V_1 I_{exc}^{\ S} \qquad \text{Eq A2}$$

where V_1 is V_{exc} at I_{exc} = 1A and S is the log-log slope of the $V_{exc,rms}$-$I_{exc,rms}$ curve as the CT goes into heavy saturation and typically has a value around 1/20. One useful result of [4] is that for a slope of 1/20:

$$\lambda_{peak} = \frac{\sqrt{2}}{\omega} V_{rms}$$

$$i_{peak} \approx 2.8\, I_{rms} \approx 2\sqrt{2} I_{rms} \quad \text{(above } V\text{-}I \text{ knee)} \qquad \text{Eq A3}$$

With this information one can quickly, though roughly, approximate a λ-I curve from a $V_{exc,rms}$-$I_{exc,rms}$ curve. The next task is to set up an equation to model the data points. The equation chosen for anhysteretic flux and permeability (μ_{anhys}) takes the form of:

$$\lambda_{anhys} = a_1 i + \frac{i}{a_2 + a_3 i} \qquad \text{Eq A4}$$

$$\mu_{i,anhys} = \frac{d\lambda_{anhys}}{di} = a_1 + \frac{(a_2)}{(a_2 + a_3 i)^2} \qquad \text{Eq A5}$$

The term involving a_1 represents the flux of an air core transformation, so it contributes appreciable flux only at very high saturation levels. The rest of the equation represents the flux of the saturable iron core. To provide an equation symmetric about the i=0 axis, for negative i the magnitude of i is used the result is adjusted accordingly.

A convenient nature of this set of equations is that one may find a first estimation of the parameters a_1, a_2, and a_3 by looking at the extremes of flux and current, as follows:

$$a_1 \approx \frac{\Delta\lambda_{sat}}{\Delta i_{sat}} \quad \left(\frac{\Delta\lambda_{sat}}{\Delta i_{sat}} \text{ is slope at } i = 10+, \text{ or when CT} \approx \text{air core xfmr} \right)$$

$$a_2 \approx \frac{1}{\left(\dfrac{\Delta\lambda_{low}}{\Delta i_{low}} \right)} \quad \left(\frac{\Delta\lambda_{low}}{\Delta i_{low}} \text{ is slope at low current and flux levels} \right)$$

$$\qquad\qquad\qquad\qquad\qquad\qquad\qquad\qquad\qquad\qquad\qquad \text{Eq A6}$$

$$a_3 \approx \frac{1}{\lambda_{sat}} \quad \left(\lambda_{sat} \text{ is flux at } i \approx 10+, \text{ or when core is fully saturated} \right)$$

Hysteresis Affect and Final Flux Equations

The hysteresis affect is the component of the λ-i curve that causes net flux to lag behind the applied H field. A detailed analysis is provided in [2]. It arises out of magnetic domains that are pinned in a given orientation by the irregular shape of magnetic domains (changing a domain's magnetization has a small physical nature). Once a sufficiently high external H field is applied, the pinning is broken and the magnetic domain becomes aligned with the external H field.

Hysteresis is modeled by skewing the equation for permeability, $d\lambda_{anhys}/di$, so that the actual rate of change is reduced till actual flux differs by some amount from the theoretical λ_{anhy}. Using a format similar to that found in [2]:

$$\mu_i = \frac{d\lambda}{di} = \left[b_1 + (1-b_1) \left(\frac{b_2 (\lambda_{anhys} - \lambda)}{\delta \lambda_{sat} - (\lambda_{anhys} - \lambda)} \right) \right] \frac{d}{di} \lambda_{anhys} \qquad \text{Eq A7}$$

where

$$\delta = +1 \, \text{if} \, \frac{di}{dt} \, \text{is} \, +, \, -1 \, \text{if} \, \frac{di}{dt} \, \text{is} \, -$$

b_1 = portion of steel that follows anhysteric curve.

b_2 = higher # forces hysteretic curve to follow λ_{anhys} more closely

CT Circuit Model and Associated Differential Equation

The differential equation for the CT circuit has the form of:

$$\frac{d}{dt} \lambda = L_2 \frac{d}{dt} i_2 + R_2 i_2$$

$$\frac{d}{dt} \lambda = \mu_i \cdot \frac{d}{dt} \left(\frac{i_1}{N} - i_2 \right) \qquad \text{Eq A8}$$

Rearranging terms yields:

$$\frac{d}{dt} i_2 = \left(\frac{1}{L_2 + u_i} \right) \left(u_i \frac{d}{dt} \frac{i_1}{N} - R_2 i_2 \right) \qquad \text{Eq A9}$$

With numerical analysis of this equation, one has the tools to determine the output of the CT for an arbitrary i_1 with a variety of software packages, and details of the work is left to a later paper.

If you have any questions or need
additional information, please contact

Basler Electric Company

Route 143, Box 269, Highland, Illinois U.S.A. 62249

Tel +1 618.654.2341 Fax +1 618.654.2351

e-mail: **info@basler.com**